*Sci*

MDPI

*Article*

# Optimizing Cyanobacterial Strain Selection for Antimicrobial Nanoparticle Synthesis: A Comprehensive Analysis

**Mónica L. Reyes-Galvis, German L. López-Barrera, Néstor A. Urbina-Suarez, Janet B. García-Martínez and Andrés F. Barajas-Solano ***

Department of Environmental Sciences, Universidad Francisco de Paula Santander, Av. Gran Colombia, No. 12E-96, Cúcuta 540003, Colombia; monicalilianaeg@ufps.edu.co (M.L.R.-G.); lucianolb@ufps.edu.co (G.L.L.-B.); nestorandresus@ufps.edu.co (N.A.U.-S.); janetbibianagm@ufps.edu.co (J.B.G.-M.)

* Correspondence: andresfernandobs@ufps.edu.co

**Abstract:** This study presents the synthesis of metal nanoparticles (NPs) with antimicrobial properties from cyanobacterial biomass. Silver (AgNP), copper (CuNP), and zinc (ZnNP) nanoparticles were prepared from exopolysaccharides (EPSs) obtained from isolated cyanobacterial strains. The antimicrobial activity of AgNPs against *Escherichia coli* and *Staphylococcus aureus* was evaluated, and compared with CuNPs and ZnNPs, AgNPs were found to have a greater capacity to inhibit bacterial growth. The main factors influencing antimicrobial activity are the concentration and type of metal used. Using an optimized experimental design, specific conditions were established to maximize the antimicrobial efficacy of the synthesized NPs. The characterization of the nanoparticles included UV–VIS, FTIR, and EDX techniques, which confirmed the formation and purity of the AgNPs. This study highlights the effectiveness of cyanobacterial EPS as a reducing and stabilizing agent and provides a sustainable and efficient alternative for producing nanoparticles with biomedical applications.

**Keywords:** metal nanoparticles; green synthesis; cyanobacteria; antimicrobial activity; silver nanoparticles; exopolysaccharides



**Citation:** Reyes-Galvis, M.L.; López-Barrera, G.L.; Urbina-Suarez, N.A.; García-Martínez, J.B.; Barajas-Solano, A.F. Optimizing Cyanobacterial Strain Selection for Antimicrobial Nanoparticle Synthesis: A Comprehensive Analysis. *Sci* **2024**, *6*, 83. https://doi.org/10.3390/sci6040083

Academic Editor: Manuel Simões

Received: 10 October 2024
Revised: 30 November 2024
Accepted: 5 December 2024
Published: 10 December 2024



## 1. Introduction

Nanotechnology has become a key area of science because of its ability to manipulate materials at the atomic and molecular levels. This has enabled the development of nanoparticles with unique properties and applications in various disciplines, including biomedicine, electronics, and materials engineering. Within this wide-ranging field of research, metal nanoparticles (NPs) have attracted considerable attention because of their exceptional physical, chemical, and biological properties, which make them suitable for antimicrobial applications. The metals most used in the synthesis of these nanoparticles are gold (Au), silver (Ag), copper (Cu), and zinc (Zn) [1], whose nanoparticles have shown effective antimicrobial activity against a wide range of microorganisms, including bacteria, viruses, and fungi.

In recent years, remarkable progress has been made in the synthesis of metal nanoparticles, accompanied by a growing interest in developing more sustainable and environmentally friendly methods [2]. The conventional synthesis of metal nanoparticles utilizes chemical processes that use toxic reducing agents and operate under harsh experimental conditions, which has led to concerns about their environmental impact and safety [3]. An alternative approach has emerged in response to these limitations: the green synthesis of metal nanoparticles. This method uses biological agents, including plant extracts, fungi, bacteria, and, more recently, cyanobacteria, to reduce metal ions to nanoparticles. Cyanobacteria, which are unicellular photosynthetic organisms that are among the oldest organisms on earth, have been identified as promising sources of biomass for the green

synthesis of metal nanoparticles because of their ability to reduce metal ions and stabilize the resulting nanoparticles [4–6].

Cyanobacteria have evolved sophisticated biochemical mechanisms over millennia to survive in extreme environments, including the ability to process heavy metals and other toxic compounds [7–9]. This ability is partly due to bioactive compounds such as proteins, polysaccharides, nucleic acids, and pigments, which can act as redox and stabilizing agents to synthesize NPs. In addition, cyanobacteria biomass can be easily cultivated under controlled conditions, providing a sustainable and renewable source to produce metal nanoparticles [10].

Metal nanoparticles (NPs) have been shown to possess antibacterial properties, the efficiency of which depends on factors such as metal type, size, shape, interaction with bacteria, and their mechanism of action. Among the most studied types of NPs are silver and copper NPs, which are known for their high antimicrobial potential. Owing to their remarkable efficacy, silver NPs are frequently used to synthesize antibacterial agents.

Previous studies have shown that NPs synthesized from algae exhibit significant antibacterial activity. For example, Ebrahiminezhad et al. [11] reported that silver nanoparticles synthesized from the microalga *Chlorella vulgaris* reduced the growth of *Staphylococcus aureus* and *Escherichia coli* by 98%. Similarly, Priyadarshini et al. [12] investigated Ag-NPs synthesized with *Scenedesmus* sp. They reported effective inhibition of various bacteria and fungi, including *E. coli*, *Vibrio cholerae*, *Streptococcus pyogenes*, *Staphylococcus aureus*, *Penicillium citrinum*, *Aspergillus flavus*, and *Candida albicans*.

Similarly, Sathishkumar et al. [13] synthesized silver nanoparticles with the microalga *Trichodesmium erythraeum* and demonstrated 100% inhibition with inhibition depths ranging from 7 to 11 mm for pathogens such as *V. cholerae*, *K. pneumoniae*, *S. aureus*, *E. coli*, and *Proteus mirabilis*. In a separate study, Silva Ferreira et al. [14] reported a 98% reduction in *S. aureus* and *K. pneumoniae* growth with silver chloride nanoparticles synthesized from *Chlorella vulgaris*. In contrast, silver nanoparticles synthesized with the cyanobacterium *Anabaena variabilis* showed remarkable antibacterial and antifungal activity. For other metals, Mandhata et al. [15] synthesized gold nanoparticles from *Anabaena spiroides* and tested them against *K. oxytoca*, *S. aureus*, and *St. pyogenes*. The results revealed excellent efficacy and confirmed the antimicrobial potential of gold.

This work investigated the synthesis of silver, copper, and zinc nanoparticles from isolated cyanobacterial strains via biomass and exopolysaccharides. In addition, the antimicrobial activity of the synthesized NPs against pathogenic bacteria such as *Escherichia coli* and *Staphylococcus aureus* was investigated. The main objective of this research is to optimize the synthesis conditions of metal nanoparticles using cyanobacteria as biofactories to maximize their antimicrobial activity and provide a more sustainable alternative to combat antibiotic-resistant microorganisms.

## 2. Materials and Methods

### 2.1. Strains

Eleven cyanobacterial strains were used in this research (Table 1). The strains were previously isolated from biofilms formed at the emergence thermal spring near the city of Cúcuta (Colombia) and kept in solid slants of BG-11 media at the INNOValgae collection (UFPS, Cucuta, Colombia) (https://www.innovalg.com (accessed on 24 September 2024)). The strains were cultured in a 1 L Schott GL45 glass flask with 0.5 L of working volume of liquid BG-11 media [16]. The strains were mixed through the constant injection of filtered air with 1% ($v/v$) $CO_2$ at a flow rate of 0.3 L/min, a photoperiod of 12:12 h (light:dark) at 100 µmol/m$^2$/s, and a temperature of 27 ± 1 °C for 15 days.

*Staphylococcus aureus* subsp. (ATCC) 25923 and *Escherichia coli* ATCC 25922 were obtained from the American Type Culture Collection and used to evaluate the antimicrobial activity of extracts from metal nanoparticles (NPs).

**Table 1.** Cyanobacterial strains present in the INNOValgae laboratory (UFPS).

| Strain Code | Orden | Genera |
|---|---|---|
| UFPS001 | *Oscillatoriales* | *Phormidium* |
| UFPS002 | *Stigonematale* | *Hapalosiphon* |
| UFPS003 | | *Potamosiphon* |
| UFPS004 | | *Leptolyngbya* |
| UFPS005 | *Oscillatoriales* | *Oscilatoria* |
| UFPS006 | | *Termoleptolyngbya* |
| UFPS007 | | *Leptolyngbya* |
| UFPS008 | *Nostocales* | *Nostoc* |
| UFPS009 | | *Nostoc* |
| UFPS010 | *Oscillatoriales* | *Potamosiphon* |
| UFPS011 | *Chroococcales* | *Chroococcus* |

### *2.2. Experimental Design for NP Synthesis and Antimicrobial Potential*

The main objective was to identify the main effect of seven factors, four numerical variables (reaction time, reaction rate, nanoparticle extract concentration, and metal salt concentration) and three categorical variables (type of metal salt, type of biomass, and strain). Therefore, an optimal (custom) design with five blocks was created in Design-Expert® software (version 22.0.2; Stat-Ease Inc., Minneapolis, MN, USA) to determine the feasibility of synthesizing metal nanoparticles from the biomass of thermotolerant cyanobacteria (Table 2). This type of design allows the analysis of the interaction between numerical and categorical variables without the need to perform many experiments with several variables. This is the first time that a single experiment aims to identify the probable interaction between several factors that has been highlighted by previous research as the most critical for NPs synthesis.

**Table 2.** Experimental design for NP synthesis.

| Factor | Name | Units | Type | SubType | Minimum | Maximum |
|---|---|---|---|---|---|---|
| A | Mixing speed | | Numeric | Continuous | 50 | 250 |
| B | time | days | | | 1 | 5 |
| C | Metal Concentration | mM | | | 0.3 | 3 |
| D | Sample-to-metal ratio | *v*/*v* | | | 1 | 10 |
| E | Type of metal | | Categoric | Nominal | $AgNO_3$ ZnO | $Cu(CH_3COO)_2{\cdot}H_2O$ |
| F | Type of sample | | | | Spent media | Biomass |
| G | Cyanobacterial strain | UFPS | | | 1 | 11 |

Biomass from a 500 mL reactor with a working volume of 300 mL was used for each experiment. The media was mixed by injecting air at an approximately 180 mL air/min flow rate. At the end of the culture period, each flask was disconnected from the airflow and allowed to acclimate for 1 h. The medium was centrifuged (3500 rpm, 20 min, 20 °C), and the spent media or the produced biomass was used according to the experimental design.

The antimicrobial activity in each experiment was analyzed via the disc diffusion method [17]. Briefly, sterilized paper discs were impregnated with different concentrations of NPs and placed in Petri dishes containing Mueller Hinton Difco™ medium (pH 7.2–7.4) previously inoculated with 100 µL of a direct suspension of colonies from either *S. aureus* subsp. (ATCC) 25923 or *E. coli* ATCC 25922 in saline adjusted to an optical density of 0.5 according to the McFarland scale for each microorganism. The plates were incubated at 37 °C for 24 h. At the end of incubation, the zone of inhibition was measured, and the data obtained were recorded.

After identifying those factors that significantly affect the synthesis of NPs and their antimicrobial potential, the next step is the reduction (proper selection) of the original design. In this case, a new design will be created using either an I-optimal, CCD, or Box–Behnken on Design-Expert® software (version 22.0.2, Stat-Ease Inc., Minneapolis,

MN, USA). This type of design is created with specialized statistical tools to optimize the response (either minimize or maximize it). Figure 1 presents a flowchart of the process.

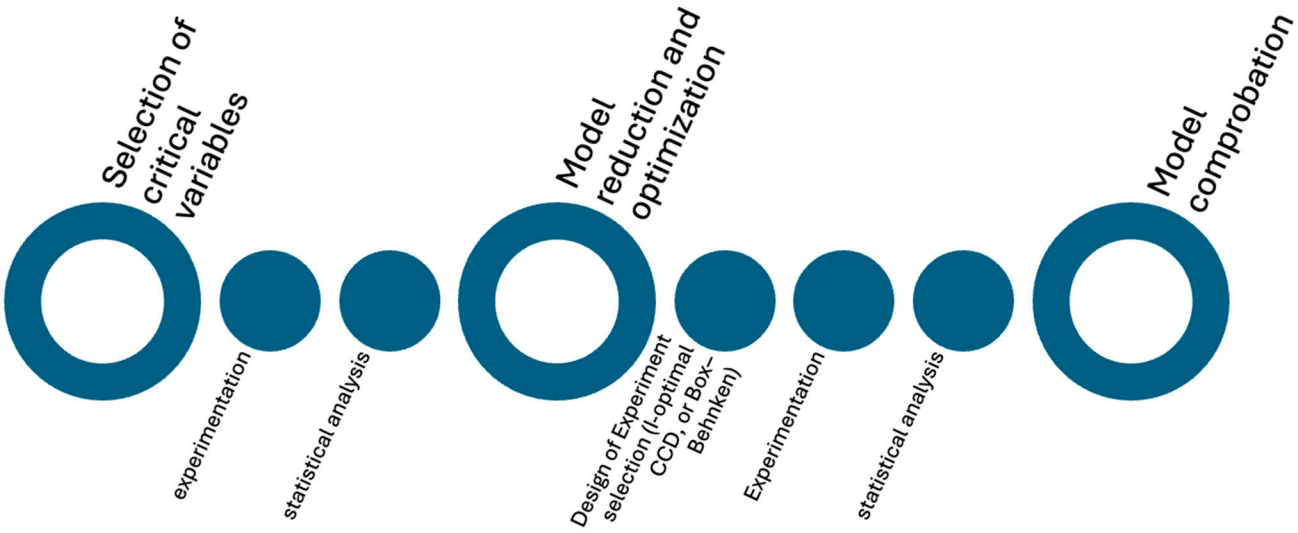


**Figure 1.** Flowchart of the proposed method to identify the most important variables for NPs synthesis using thermotolerant cyanobacteria.

### *2.3. Experimental Design for NP Synthesis and Antimicrobial Potential*

The techniques used for this characterization included UV–VIS, FTIR, and EDX, which are based on previous methods by Mandhata [15], Roychoudhury [18], and Vanlalveni [19].

#### 2.3.1. UV–VIS Characterization

The initial and final UV–VIS measurements were performed via a Spectroquant Pharo 300 UV/VIS spectrophotometer (Merck KGaA, Darmstadt, Germany) in the range of 200–800 nm to analyze the maximum absorbances of the samples.

#### 2.3.2. EDX Characterization

The chemical composition of the produced NPs was determined via energy-dispersive X-ray spectroscopy (EDX) via a Phenom ProX electron microscope. This confirmed the presence of silver and other elements.

#### 2.3.3. FTIR Characterization

To identify the functional groups of the produced NPs, FTIR spectra were recorded via a JASCO FT/IR-6800 type A spectrometer with an ATR support, covering the range of 400–4500 $cm^{-1}$.

## 3. Results

*Evaluation of Operational Factors for the Synthesis of Metallic NPs*

Seven key variables were evaluated for synthesizing metal nanoparticles (Ag, Cu, and Zn) with antimicrobial capacity: stirring speed, stirring time, metal concentration, algae-to-metal ratio, metal type, sample type, and strain used. A D-optimal response surface experimental design was used to identify the factors with the greatest influence on antimicrobial activity against *Staphylococcus aureus* and *Escherichia coli*. The most critical factors were the metal concentration and type, with silver ($AgNO_3$) resulting in the highest antimicrobial activity (Table 3).

For *S. aureus*, the statistical model was significant (F value of 11.27, $p$ value < 0.0001), indicating the following optimal operating conditions: agitation speed of 233 rpm, time of 4.17 days, metal concentration of 2.93 mM and algae-to-metal ratio of 4.58% $v/v$. The NPs were synthesized via cell-free medium (EPS) and strain UFPS006.

**Table 3.** ANOVA results and linear model for *Staphylococcus aureus* subsp. ATCC 25923.

| | Source | Sum of Squares | Df | Mean Square | F Value | *p* Value |
|---|---|---|---|---|---|---|
| | Block | 26.72 | 4 | 6.68 | | |
| | Model | 210.94 | 16 | 13.18 | 11.27 | <0.0001 * |
| A | 2.97 | 1 | 2.97 | 2.54 | 0.1163 ** | 0.1749 ** |
| B | 0.6252 | 1 | 0.6252 | 0.5345 | 0.4675 ** | 0.7796 ** |
| C | 12.54 | 1 | 12.54 | 10.72 | 0.0017 * | 0.0038 * |
| D | 0.1259 | 1 | 0.1259 | 0.1076 | 0.7440 ** | 0.4631 ** |
| E | 173.70 | 1 | 173.70 | 148.48 | <0.0001 * | <0.0001 * |
| F | 1.54 | 1 | 1.54 | 1.32 | 0.2551 ** | 0.3939 ** |
| G | 17.49 | 10 | 1.75 | 1.50 | 0.1624 ** | 0.0685 ** |
| | Residual | 43.70 | 63 | 0.69 | | |
| | Lack of fit | 43.66 | 61 | 0.72 | 6.77 | 0.2161 ** |
| | Pure error | 0.0391 | 2 | 0.0196 | | |
| | **Cor Total** | 281.37 | 83 | | | |

| **Std. Dev** | **Mean** | **C.V%** | **$R^2$** | **$R^2$ adj** | **$R^2$ Pred** | **Adq Pr** |
|---|---|---|---|---|---|---|
| 1.08 | 1.54 | 70.44 | 0.7411 | 0.6753 | 0.5330 | 10.6568 |

* Significant, ** Not significant.

Similar results were obtained for *E. coli* with a significant statistical model (F value of 13.41, *p* value < 0.0001). The optimal conditions for maximizing antimicrobial activity were a mixing speed of 244 rpm, a time of 2.68 days, a metal concentration of 2.88 mM, and an algae-to-metal ratio of 8.27% *v*/*v*, with the use of $AgNO_3$, and *Chroococcus*_UFPS011 cell-free medium (Table 4).

**Table 4.** ANOVA results and a linear model for *Escherichia coli* ATCC 25922.

| | Source | Sum of Squares | Df | Mean Square | F Value | *p* Value |
|---|---|---|---|---|---|---|
| | Block | 9.04 | 4 | 2.26 | | |
| | Model | 106.41 | 16 | 6.65 | 13.41 | <0.0001 * |
| A | Mixing speed | 0.9336 | 1 | 0.9336 | 1.88 | 0.1749 ** |
| B | time | 0.0392 | 1 | 0.0392 | 0.0790 | 0.7796 ** |
| C | Metal Concentration | 4.48 | 1 | 4.48 | 9.04 | 0.0038 * |
| D | Sample-to-metal ratio | 0.2702 | 1 | 0.2702 | 0.5449 | 0.4631 ** |
| E | Type of metal | 92.61 | 1 | 92.61 | 186.78 | <0.0001* |
| F | Type of sample | 0.3654 | 1 | 0.3654 | 0.7369 | 0.3939 ** |
| G | Cyanobacterial strain | 9.21 | 10 | 0.9212 | 1.86 | 0.0685 ** |
| | Residual | 31.24 | 63 | 0.4958 | | |
| | Lack of fit | 30.99 | 61 | 0.5081 | 4.15 | 0.2134 ** |
| | Pure error | 0.2448 | 2 | 0.1224 | | |
| | **Cor Total** | 146.69 | 83 | | | |

| **Std. Dev** | **Mean** | **C.V%** | **$R^2$** | **$R^2$ Adj** | **$R^2$ Pred** | **Adq Pres** |
|---|---|---|---|---|---|---|
| 0.7024 | 1.09 | 64.87 | 0.7731 | 0.7154 | 0.5840 | 12.3057 |

* Significant, ** Not significant.

After the most statistically significant factors that enhance the synthesis of NPs and their antimicrobial activity on *S. aureus* and *E. coli* were identified, a new experimental design focused on optimizing the antimicrobial activity, a central composite design, was chosen as the most suitable option because of the reduced number of variables. In this case, a central composite design of three factors, three blocks, and twenty runs was created on Design-Expert® software (version 22.0.2, Stat-Ease Inc., Minneapolis, MN, USA) separately for *S. aureus* and *E. coli* (Table 5).

*Chroococcus*_UFPS011 was grown in a 500 mL flask with a working volume of 300 mL of BG-11 culture media for each experiment. The media was mixed by injecting air at an approximately 180 mL air/min flow rate. At the end of the culture period, each flask was disconnected from the airflow and allowed to acclimate for 1 h. The medium was

centrifuged (3500 rpm, 20 min, 20 °C), and the spent media or the produced biomass was used according to the experimental design.

**Table 5.** CCD for *S. aureus* and *E. coli*.

| Microbial Sample | Factor | Name | Units | Type | $-\alpha$ | Low | Medium | High | $+\alpha$ |
|---|---|---|---|---|---|---|---|---|---|
| *S. aureus* | A | Time | days | Numeric | −1.39 | 1 | 4.5 | 8 | 10.39 |
| | B | Metal Concentration | mM | | −0.3636 | 1 | 3 | 5 | 6.36 |
| | C | Sample-to-metal ratio | *v*/*v* | | −1.39 | 1 | 4.5 | 8 | 10.39 |
| *E. coli* | A | Time | days | Numeric | −0.3636 | 1 | 3 | 5 | 6.36 |
| | B | Metal Concentration | mM | | −0.3636 | 1 | 3 | 5 | 6.36 |
| | C | Sample-to-metal ratio | *v*/*v* | | −2.09 | 2 | 8 | 14 | 18.09 |

The results of the ANOVA of the antimicrobial capacity of the $AgNO_3$ nanoparticles against *S. aureus* are presented in Table 6. According to the results, the proposed model is statistically significant because the F value (262.5) and *p* value (<0.0001) are reported. In the case of *S. aureus*, the metal concentration and sample-to-metal ratio are the factors with the greatest influence on antimicrobial ability. Notably, several interactions between factors such as AC, BC, and AB and all squared factors ($A^2$, $B^2$, and $C^2$) were significant. This finding indicates that the model fits a quadratic system. On the other hand, the $R^2$ squared obtained for the new model is not only statistically significant but also higher than that of the first design (from 0.7 to 0.99), which denotes a significant improvement in the quality of the results. Finally, the inherent noise (adequate precision) of the experimental phase is minimal compared with that of the signal.

**Table 6.** ANOVA results for optimized AgNPs for *Staphylococcus aureus* subsp. ATCC 25923.

| | Source | Sum of Squares | Df | Mean Square | F Value | *p* Value |
|---|---|---|---|---|---|---|
| | Block | 1.01 | 2 | 0.5063 | | |
| | Model | 33.23 | 9 | 3.69 | 262.50 | <0.0001 * |
| A | Time | 0.0637 | 1 | 0.0637 | 4.53 | 0.0659 ** |
| B | Metal Concentration | 2.44 | 1 | 2.44 | 173.14 | <0.0001 * |
| C | Sample-to-metal ratio | 0.2799 | 1 | 0.2799 | 19.90 | 0.0021 * |
| | AB | 0.1037 | 1 | 0.1037 | 7.37 | 0.0265 * |
| | AC | 0.2220 | 1 | 0.2220 | 15.79 | 0.0041 * |
| | BC | 4.14 | 1 | 4.14 | 294.15 | <0.0001 * |
| | $A^2$ | 6.64 | 1 | 6.64 | 472.25 | <0.0001 * |
| | $B^2$ | 14.27 | 1 | 14.27 | 1014.47 | <0.0001 * |
| | $C^2$ | 10.03 | 1 | 10.03 | 713.37 | <0.0001 * |
| | Residual | 0.1125 | 8 | 0.0141 | | |
| | Lack of Fit | 0.0811 | 5 | 0.0162 | 1.55 | 0.3811 ** |
| | Pure Error | 0.0314 | 3 | 0.0105 | | |
| | **Cor Total** | 34.35 | 19 | | | |

| **Std. Dev** | **Mean** | **C.V%** | **$R^2$** | **$R^2$ Adj** | **$R^2$ Pred** | **Adq Pres** |
|---|---|---|---|---|---|---|
| 0.1186 | 2.07 | 5.72 | 0.9966 | 0.9928 | 0.9745 | 43.6078 |

* Significant, ** Not significant.

The response surface for the antimicrobial activity of the nanocomposite is shown in Figure 2. In the figure, it is possible to appreciate the conical shape of the surface, where it is possible to highlight a zone with a higher response (in mm of inhibition) and zones in the corners with a lower response; this conical response allows us to correctly identify a maximization zone in the center of the design, in which medium concentrations of the algae–metal ratio and high concentrations of $AgNO_3$ present the best results.

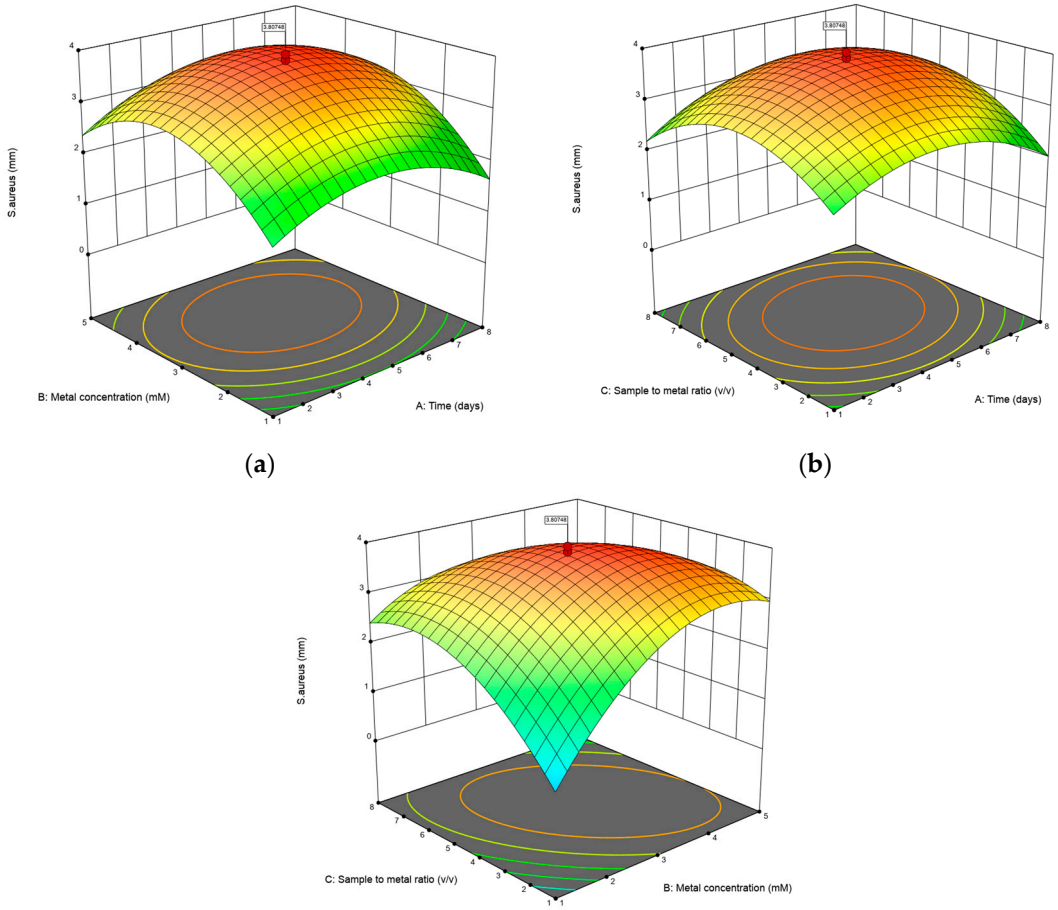


**Figure 2.** Surface response of *S. aureus* to the antimicrobial activity of *AgNPs*. (**a**) Interaction between the metal concentration and time; (**b**) interaction between the sample-to-metal ratio and time; (**c**) interaction between the sample-to-metal ratio and the metal concentration.

The results of the ANOVA of the antimicrobial ability of the AgNPs against *E. coli* are presented in Table 7. According to the results, the proposed model is statistically significant because of the F value (213.26) and *p* value (<0.0001). The most influential factors were time, metal concentration, and algae-metal concentration. Notably, several interactions between factors such as BC and all squared factors ($A^2$, $B^2$, and $C^2$) were significant. This finding indicates that the model fits a quadratic system. On the other hand, the $R^2$ squared obtained for the new model is not only statistically significant but also higher than that of the first design (from 0.7 to 0.99), which denotes a significant improvement in the quality of the results. Finally, the inherent noise (adequate precision) of the experimental phase is minimal compared with that of the signal.

The response surface for the antimicrobial activity of the nanocomposite is shown in Figure 3. In the figure, it is possible to appreciate the conical shape of the surface, where it is possible to highlight an elevated area (red color), where the expected response is higher in comparison with the lower parts of the surface (green color); this form enables us to accurately locate a maximizing zone in the middle of the design, where the greatest outcomes are produced by medium quantities of the algae–metal ratio and high concentrations of $AgNO_3$.

Considering these findings, the best operating conditions for maximizing the antimicrobial capacity of the AgNPs for both *S. aureus* and *E. coli* were obtained (Table 8).

**Table 7.** ANOVA results for optimized AgNPs from *Escherichia coli* ATCC 25922.

| | Source | Sum of Squares | Df | Mean Square | F Value | *p* Value |
|---|---|---|---|---|---|---|
| | Block | 0.6761 | 2 | 0.3381 | | |
| | Model | 36.70 | 9 | 4.08 | 213.26 | <0.0001 * |
| A | Time | 0.4791 | 1 | 0.4791 | 25.06 | 0.0010 * |
| B | Metal Concentration | 2.70 | 1 | 2.70 | 140.96 | <0.0001 * |
| C | Sample-to-metal ratio | 1.27 | 1 | 1.27 | 66.16 | <0.0001 * |
| | AB | 0.0328 | 1 | 0.0328 | 1.71 | 0.2269 ** |
| | AC | 0.0046 | 1 | 0.0046 | 0.2410 | 0.6367 ** |
| | BC | 0.7021 | 1 | 0.7021 | 36.72 | 0.0003 * |
| | $A^2$ | 9.54 | 1 | 9.54 | 499.09 | <0.0001 * |
| | $B^2$ | 12.95 | 1 | 12.95 | 677.41 | <0.0001 * |
| | $C^2$ | 15.22 | 1 | 15.22 | 795.81 | <0.0001 * |
| | Residual | 0.1530 | 8 | 0.0191 | | |
| | Lack of Fit | 0.1119 | 5 | 0.0224 | 1.64 | 0.3638 ** |
| | Pure Error | 0.0411 | 3 | 0.0137 | | |
| | **Cor Total** | 37.53 | 19 | | | |

| **Std. Dev** | **Mean** | **C.V%** | **$R^2$** | **$R^2$ Adj** | **$R^2$ Pred** | **Adq Pres** |
|---|---|---|---|---|---|---|
| 0.1383 | 1.86 | 7.43 | 0.9958 | 0.9912 | 0.9773 | 36.7342 |

* Significant, ** Not significant.

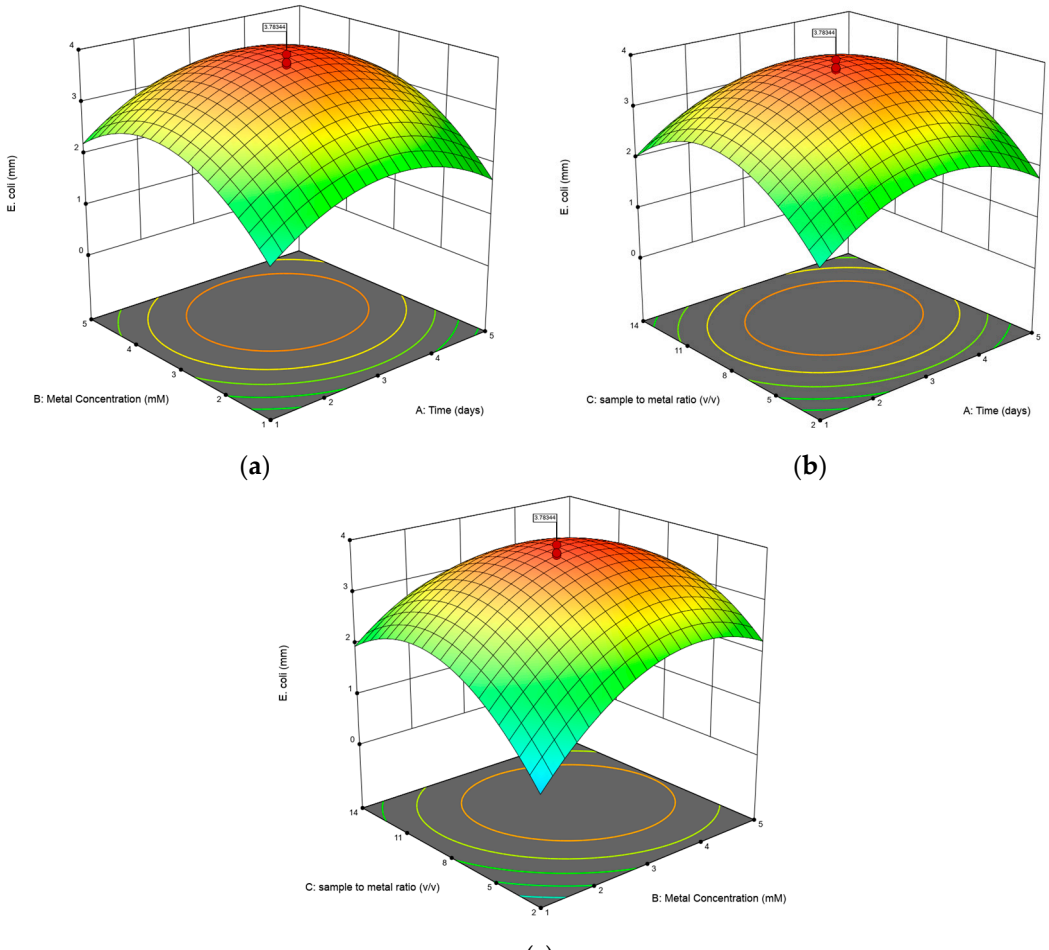


**Figure 3.** Surface response of the antimicrobial activity of AgNPs toward *E. coli*. (**a**) Interaction between the metal concentration and time; (**b**) sample-to-metal ratio and time; (**c**) sample-to-metal ratio and metal concentration.

**Table 8.** Optimized conditions for AgNP synthesis.

| Microbial Sample | Factor | Name | Units | Value |
|---|---|---|---|---|
| *S. aureus* | A | Time | days | 4.5 |
| | B | Metal Concentration | mM | 3 |
| | C | Sample-to-metal ratio | $v/v$ | 4.5 |
| | $Z_1$ | Inhibition halo (expected) | mm | 3.48 |
| *E. coli* | A | Time | days | 3 |
| | B | Metal Concentration | mM | 3 |
| | C | Sample-to-metal ratio | $v/v$ | 8 |
| | $Z_2$ | Inhibition halo (expected) | mm | 3.64 |

The new AgNPs were synthesized according to previously obtained conditions (Table 8) and were used to determine their antimicrobial capacity against *S. aureus* and *E. coli*. The expected inhibition value was analyzed against the experimentally observed value for each nanocomposite (in triplicate) to achieve the above. The data were analyzed via a one-sample t test in GraphPad Prism version 10.3.1 for Mac (GraphPad Software, Boston, MA, USA; www.graphpad.com, accessed on 18 November 2024).

According to the *t* test results for the observed data (Figure 4), the obtained nanocomposites present a statistically greater value than that expected by the CCD model. This shows good replicability of the experimental conditions obtained, so it is possible to obtain nanocomposites using the postculture medium of thermotolerant cyanobacteria as a matrix.

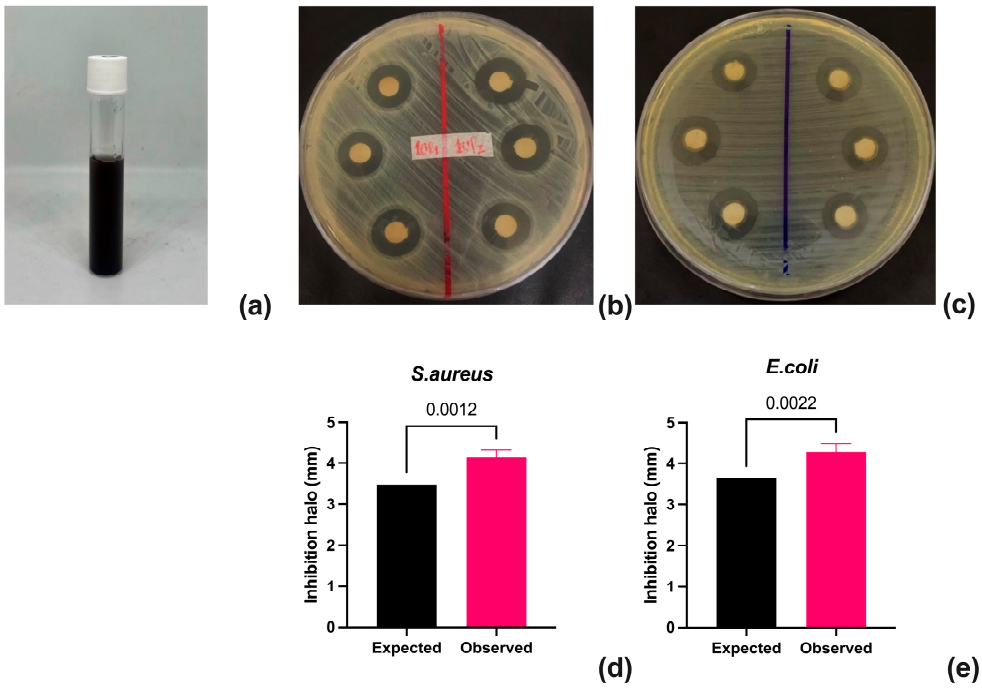


**Figure 4.** Confirmation of the antimicrobial activity of synthesized AgNPs. (**a**) Synthesized AgNPs; (**b**) inhibition halo for *S. aureus*; (**c**) inhibition halo for *E. coli*; (**d**) expected vs. observed analysis of the inhibition halo for *S. aureus*; (**e**) expected vs. observed analysis of the inhibition halo for *E. coli*.

Since the cell-free consumed culture medium showed a better capacity for the synthesis of NPs than the biomass produced, it was necessary to determine the composition of the possible extracellular metabolites, since cyanobacteria are recognized as producers of exopolymeric material (EPS) in the culture medium; therefore, the medium was used to determine the content of total carbohydrates [20], total proteins [21], and total lipids [22]. The results of their characterization are presented in Figure 5. According to the data, the concentrations of carbohydrates, proteins, and total lipids between the two strains analyzed

were significantly different; however, the most significant differences were found in the concentrations of total proteins and total lipids.

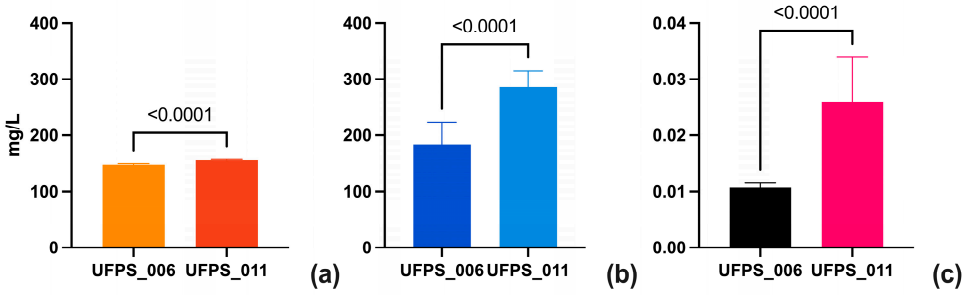


**Figure 5.** Macromolecules in the spent culture media of strains UFPS006 and UFPS011. (**a**) Total carbohydrates; (**b**) total proteins; (**c**) total lipids.

The UV–VIS spectra of the AgNP extracts were recorded with a Spectroquant Pharo 300 UV/VIS spectrophotometer (Figure 6) in the wavelength range from 200 to 800 nm. Initially, the formation of AgNPs could be detected with the naked eye by changing color from translucent to dark pink. The highest absorbance was obtained at a wavelength of 427 nm for AgNP006 and 438 nm for AgNP011 (Figure 6), indicating the formation of AgNPs. The wavelengths between 400 and 450 nm are the typical range of maximum wavelengths for AgNPs and can be attributed to spherical NPs [23].

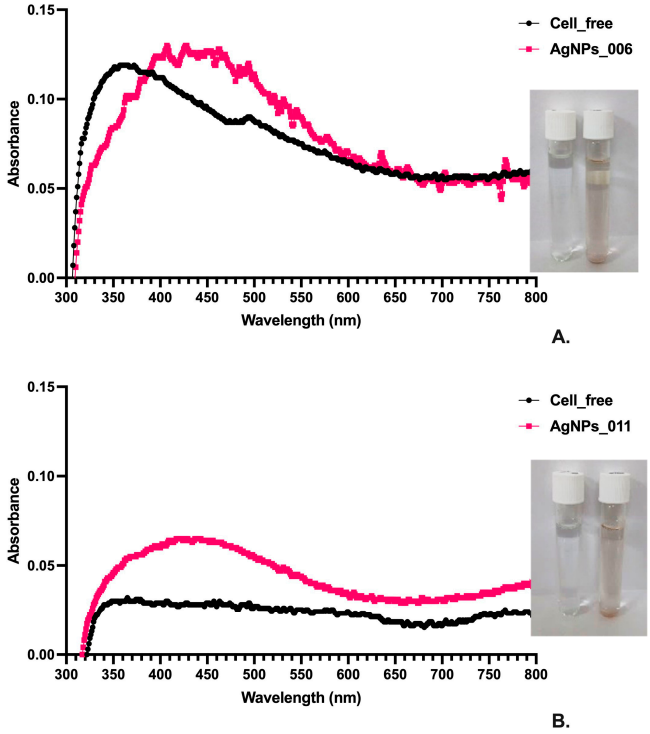


**Figure 6.** UV–VIS characterization of (**A**) AgNP006 and (**B**) AgNP011.

EDX analysis confirmed the presence of silver and other elements in the synthesized NPs with purities higher than 74%. The chemical composition was consistent with the literature and included carbon, oxygen, aluminum, and potassium in the AgNPs (Figure 7).

Figure 8 shows the FTIR spectra of the two synthesized nanoparticles (NPs), with observed peaks around 3500, 2900, 2200, 1600, 1200, 1000, 900, 800, and 460 $cm^{-1}$. Peaks in the 3200–3600 $cm^{-1}$ range are attributed to O-H and N-H stretching vibrations from polysaccharides and proteins involved in AgNP synthesis [24,25]. The peak between 2800 and 3000 $cm^{-1}$ corresponds to C-H stretching in alkane groups, while the range of 2100–2300 $cm^{-1}$ is assigned

to C≡C stretching vibrations of alkynes. Peaks at 1400–1600 $cm^{-1}$ reflect C=C group stretching vibrations and N-H bending from protein amines [26]. Vibrations in the 800–1300 $cm^{-1}$ range are linked to C-O or C-N bond stretching in ethers and amines, while those between 400 and 800 $cm^{-1}$ correspond to the interaction of silver nanoparticles with hydroxyl groups [27].

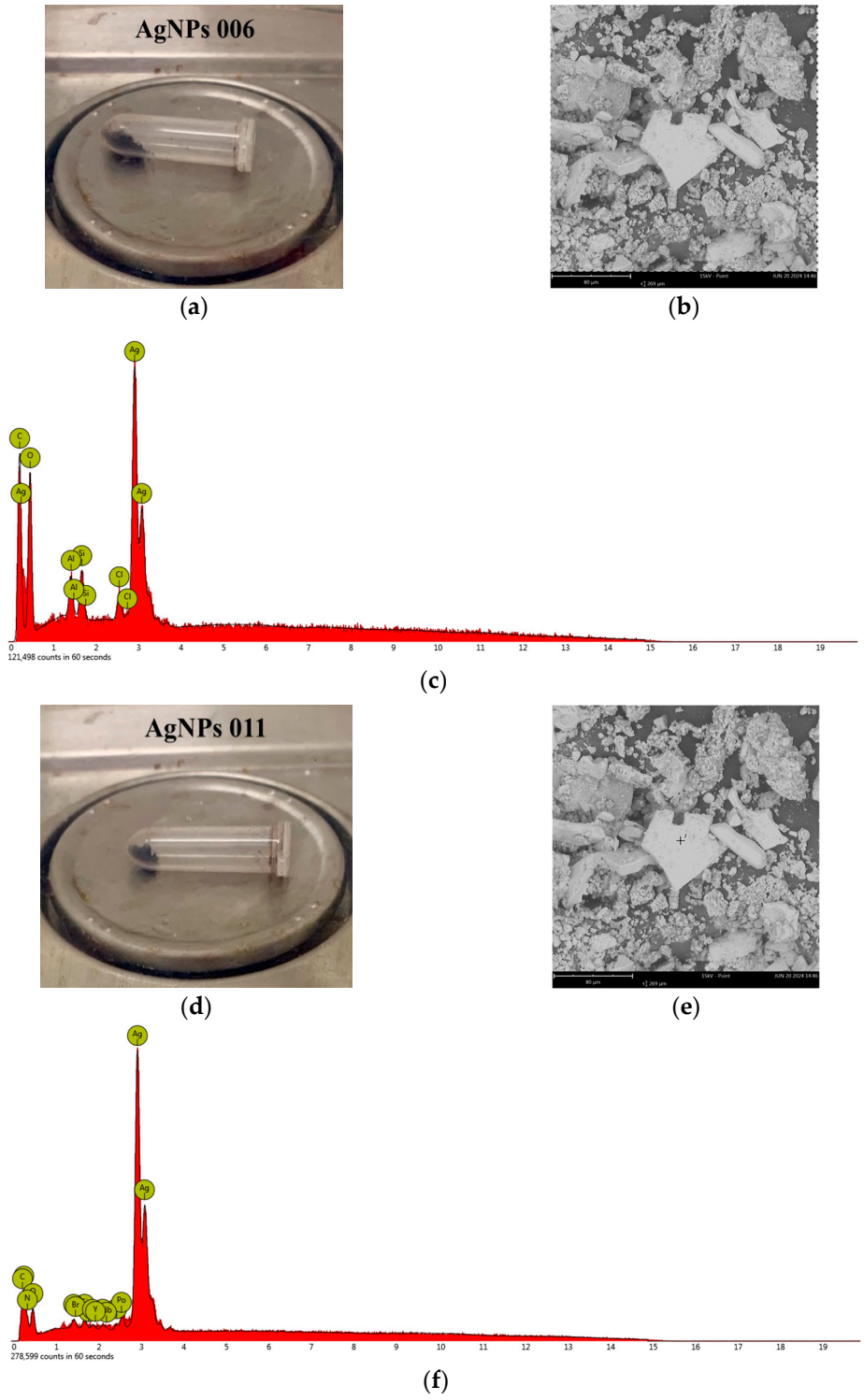


**Figure 7.** SEM and EDX characterization of AgNP006; and AgNP011. (**a**) Macroscopic image, (**b**) SEM, and (**c**) EDX analysis of AgNP006, (**d**) Macroscopic image, (**e**), SEM, and (**f**) EDX analysis of AgNP011.

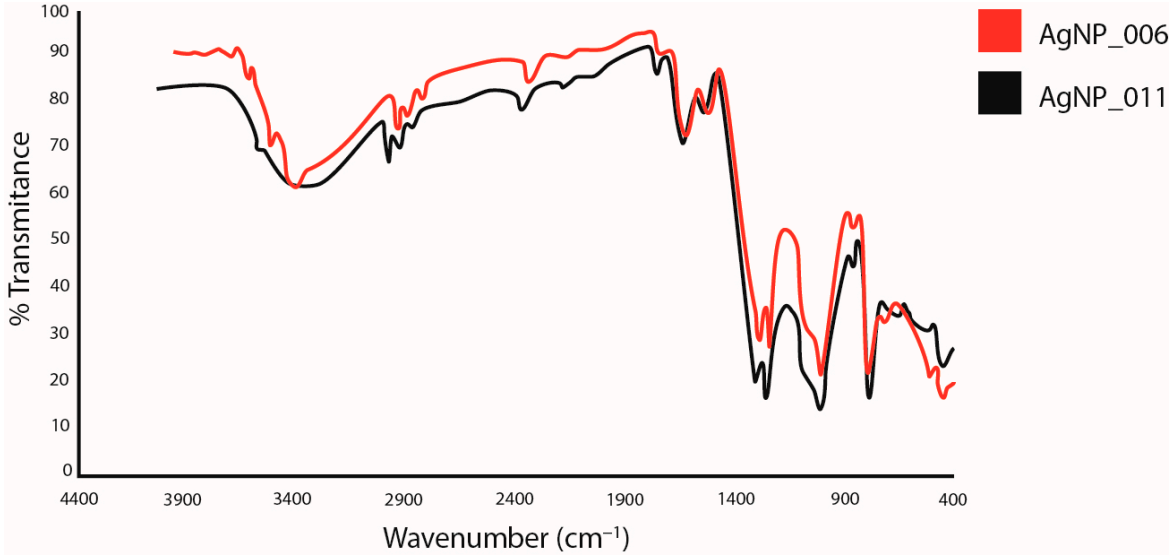


**Figure 8.** FIT-IR characterization of AgNP006 and AgNP011.

The FTIR data indicate the presence of amide and hydroxyl functional groups in proteins and polysaccharides, which could act as reducing agents for silver ions to AgNPs. These results align with findings from recent studies suggesting that biomolecules in exopolysaccharides facilitate silver ion reduction, possibly via enzymatic catalysis by nitrate reductase [24,28,29].

## 4. Discussion

In the context of nanoparticle synthesis, ANOVA revealed that the concentration and type of metal were the most influential factors in obtaining nanoparticles with antimicrobial activity. Silver nanoparticles (AgNPs) demonstrated average inhibition zones of 4 mm, significantly larger than those of copper (CuNPs) and zinc nanoparticles (ZnNPs), which exhibited minimal or no activity. These findings align with previous studies highlighting silver's superior antimicrobial properties due to its ability to denature proteins and induce cellular dysfunction in bacteria [30]. For instance, Kohsari et al. [31] showed that AgNPs synthesized via biological methods have a heightened antimicrobial impact, particularly against *S. aureus* and *E. coli*, by disrupting bacterial cell membranes, confirming the superiority of silver over other metals. Similarly, Huq [32] noted that silver nanoparticles offer greater stability and antimicrobial efficacy than zinc oxide nanoparticles, primarily due to AgNPs' ability to generate reactive oxygen species (ROS).

The antimicrobial efficacy of AgNPs was greater against Gram-positive bacteria than Gram-negative bacteria, owing to structural differences in bacterial membranes. Gram-positive bacteria have a single cell membrane surrounded by a thick peptidoglycan layer, which allows nanoparticle penetration and antimicrobial effects. In contrast, Gram-negative bacteria possess an outer membrane rich in lipopolysaccharides, acting as a barrier that restricts the penetration of larger particles such as AgNPs [33]. This trend was also highlighted by Manosalva [34] who observed that bacterial membrane structures directly influence nanoparticle effectiveness. Complementary findings by Vidovic et al. [35] indicated that zinc nanoparticles exhibit greater metabolic effects due to the vulnerability of Gram-negative transmembrane proteins to zinc.

Cyanobacterial biomass and their exopolysaccharides (EPS) have proven highly effective for the synthesis and stabilization of silver nanoparticles (AgNPs). Due to their inherent nature and functionality, these biopolymers act as reducing and stabilizing agents, facilitating the formation of stable nanoparticles with enhanced antimicrobial properties [36]. For example, Shaaban et al. [37] demonstrated that using Streptomyces strains improves the synthesis of zinc oxide and silver nanoparticles, highlighting that EPS reduces variability in nanoparticle

size and shape, thereby enhancing antimicrobial activity. Furthermore, Gao et al. [38] reported that combining silver nanoparticles with antimicrobial peptides not only enhances their antimicrobial efficacy but also prolongs their stability in complex biological environments. In the medical context, recent studies have revealed that EPS-based nanoparticles also exhibit antitumor, antiviral, and antioxidant properties, as observed in *Chlorella vulgaris*, broadening their therapeutic applications [39].

The statistical analysis of ANOVA values provides critical insights into the reliability of the model. An adjusted $R^2$ of 0.6753 for S. aureus and 0.7154 for *E. coli* indicates that the model explains a moderate proportion of the observed variability. Comparatively, Singh [40] suggested that an $R^2$ above 80% is necessary for highly predictive models in nanoparticle synthesis. However, Tufail et al. [41] emphasized that an $R^2$ in the range of 70–75% can be acceptable for complex systems where inherent variability is difficult to control.

The non-significant lack of fit ($p > 0.05$) in both models indicates that the model adequately captures experimental variability while minimizing systematic errors. This aligns with the findings of wypij [42], who stressed the importance of low lack-of-fit values for validating models in antimicrobial nanoparticle synthesis. Conversely, Rai et al. [43] noted that including nonlinear interactions could improve the precision of models where size variability affects antimicrobial activity. The significant F value ($F = 11.27$, $p < 0.0001$) confirms that the proposed model explains the data better than residual error. Studies by Niranjan [44] similarly observed that high F values are associated with the strong influence of parameters such as metal concentration and reaction time on antimicrobial activity. Additionally, Medina Cruz et al. [45] found that models with high F values directly correlate with smaller nanoparticle sizes and enhanced biological stability, which supports their antimicrobial effectiveness. AgNPs (silver nanoparticles) are emerging as promising tools against bacterial infections, supported by their efficacy against Gram-positive bacteria and their applications in biomedicine, including antitumor therapies [46,47].

The central composite design (CCD) played a pivotal role in this study by optimizing the experimental conditions to maximize the antimicrobial activity of silver nanoparticles (AgNPs). This statistical approach enabled precise modeling and analysis of interactions between critical variables such as silver nitrate concentration ($AgNO_3$), reaction time, and the algae-to-metal ratio. The results, depicted in the response surface plots (Figures 1 and 2), indicated that optimal conditions included moderate $AgNO_3$ concentrations (approximately 2.9 mM) and specific algae-to-metal ratios (4.58% $v/v$ for *S. aureus* and 8.27% $v/v$ for *E. coli*). These combinations maximized bacterial inhibition zones, as detailed in Table 3 and Figure 4d,e, validating the model's efficacy.

The CCD demonstrated its utility not only in identifying optimal individual parameters but also in elucidating complex interactions that directly impact antimicrobial performance. For instance, Figures 2a–c and 3a–c illustrate that the interaction between reaction time and the algae-to-metal ratio plays a crucial role in the morphology and stability of synthesized nanoparticles. This behavior aligns with recent studies, such as Nikaeen et al. [48], which showed that CCD effectively optimizes AgNP biosynthesis through precise adjustments in reactant proportions and reaction conditions. In this study, optimization not only enhanced antimicrobial activity but also ensured greater nanoparticle stability, both of which are critical factors for industrial applications.

Furthermore, the F and $p$ values reported in Table 3 reinforce the statistical significance of interactions among the variables. The model demonstrated a strong predictive ability for expected antimicrobial responses, with a significant correlation between predicted and observed values. Similar studies, such as Elshafel et al. [49], have emphasized the utility of CCD in optimizing biological processes, noting that this statistical approach minimizes experimental variability and maximizes reproducibility. This is particularly relevant in nanoparticle synthesis, where minor variations in reaction conditions can significantly impact the final product's properties.

A detailed analysis of the response surfaces also revealed how algae-to-metal ratios influence nanoparticle antimicrobial activity. For example, Figure 3a,b show that suboptimal ratios significantly reduce bactericidal efficacy, underscoring the importance of precise balance among components. These findings are consistent with Padilla-Cruz et al. [50] who observed that proper reactant ratios and reaction conditions are critical for producing homogeneous nanoparticles with high antimicrobial activity.

The use of biological media, such as exopolysaccharides (EPS), further adds a sustainable dimension to the synthesis process. As referenced in other studies [36,39], these biopolymers contain functional groups that facilitate the reduction in metal ions and stabilize nanoparticles by preventing aggregation. This green approach not only minimizes environmental impact but also enhances the quality and uniformity of the final product. In an industrial context, combining CCD with biological methods offers a powerful tool for implementing sustainable and reproducible nanomaterial synthesis processes. By identifying and optimizing key parameters through CCD, the process ensures not only antimicrobial efficacy but also economic feasibility and scalability. Recent studies, such as Adibah et al. [51], have highlighted that advanced statistical methods like CCD are essential for designing nanoparticles with specific properties tailored for medical and technological applications.

The UV-VIS spectra recorded for silver nanoparticle (AgNP) extracts corresponding to the UFPS006 and UFPS011 strains showed characteristic absorption peaks at 427 nm and 438 nm, respectively, as illustrated in Figure 6. These values confirm the formation of spherical silver nanoparticles, as these wavelengths fall within the typical range for surface plasmon resonance (400–450 nm) associated with spherical metallic nanoparticles [18,19,23]. The differences in absorption peaks between strains likely reflect variations in the size and morphology of the synthesized nanoparticles, which may be attributed to biochemical differences in the exopolysaccharides (EPS) secreted by each strain. These biomolecules, containing functional groups such as hydroxyl, amine, and carboxyl groups, interact with silver ions during synthesis, modulating both nanoparticle growth and stability.

In this context, the observed color change in the solutions, from transparent to dark pink, served as an initial visual indicator of nanoparticle formation. This phenomenon, which reflects the intensity of surface plasmon resonance, is also related to particle concentration, size, and distribution. Recent studies, such as that by Aletayeb et al. [52], have noted that EPS not only reduce and stabilize nanoparticles but also influence their optical and structural properties. For instance, nanoparticles synthesized with EPS-rich extracts exhibited smaller sizes and greater uniformity, enhancing their antimicrobial functionality. Moreover, the differences observed between the 427 nm and 438 nm peaks for the UFPS006 and UFPS011 strains could be linked to the biochemical factors influencing nanoparticle nucleation and growth. In this regard, Ispirli et al. [53] demonstrated that EPS extracted from different bacterial strains not only stabilize nanoparticles but also affect their size and antimicrobial capacity due to specific interactions between the functional groups of EPS and metal ions. Additionally, Nilavukkarasi et al. [54] emphasized that modulating parameters such as the initial silver nitrate concentration and pH can fine-tune nanoparticle properties, maximizing their efficiency in antimicrobial applications. UV-VIS analysis not only validates nanoparticle formation but also provides critical insights for optimizing synthesis conditions. Studies such as that by Hamouda et al. [55] have highlighted that the optical properties obtained from UV-VIS spectra are key indicators of nanoparticle quality. For example, nanoparticles synthesized with chemically modified EPS showed more defined absorption peaks and greater colloidal stability, underscoring the importance of this analysis for process control in nanoparticle synthesis.

The EDX analysis of silver nanoparticles (AgNPs) synthesized using UFPS006 and UFPS011 strains revealed a purity exceeding 74%, with prominent silver peaks and traces of other elements such as carbon, oxygen, aluminum, and potassium (Figure 7). These results reflect the efficacy of cyanobacteria-based synthesis, positioning this method as a viable alternative to traditional approaches. Compared to previous studies reporting purities between 24% and 49%, the higher levels observed here emphasize the potential of

thermotolerant cyanobacteria to produce nanoparticles with superior chemical quality [56]. The presence of oxygen, attributed to residual organic compounds from the culture medium or oxidation processes, highlights the role of exopolysaccharides (EPS) in nanoparticle stabilization. This finding aligns with Hanna et al. [56], who reported that EPS not only facilitate metal ion reduction but also influence the chemical composition of nanoparticles, enhancing their stability.

The elemental composition underscores the active interaction between EPS secreted by cyanobacteria and silver ions. Acting as reducing and stabilizing agents, EPS prevent nanoparticle aggregation and promote uniformity and functionality. This aligns with Karageorgou et al. [57], who demonstrated that cyanobacterial EPS yield smaller nanoparticles with enhanced antimicrobial activity—critical features for biomedical applications. Additionally, the ability of EPS to modulate nanoparticle properties contributes to the sustainability of the synthesis process by minimizing chemical waste. Trace elements such as aluminum and potassium may originate from the culture medium or specific synthesis conditions. Though present in small amounts, these elements can influence nanoparticle colloidal stability. Sahoo et al. [58] reported that incorporating trace elements into biologically synthesized nanoparticles enhanced their ability to interact with bacterial membranes, thereby increasing antimicrobial activity. This underscores the importance of stringent control over culture parameters to ensure a homogeneous and functional final product.

The high purity of these nanoparticles not only enhances their antimicrobial activity but also makes them suitable for biomedical applications. For instance, Guna Swetha et al. [59] indicated that high-purity nanoparticles pose lower cytotoxicity risks, making them ideal candidates for medical devices and antimicrobial coatings. Furthermore, their chemical stability positions them as an effective solution against multidrug-resistant bacteria. Younis et al. [60] reported that biologically synthesized nanoparticles exhibit high efficacy against multidrug-resistant strains. Finally, the use of sustainable methods, such as reusing post-culture media, offers significant environmental benefits. This approach not only reduces production costs but also minimizes reliance on toxic chemical reagents, contributing to a circular economy.

The results of this research highlight the effectiveness of metal nanoparticles (NPs), mainly silver nanoparticles (AgNPs) synthesized from cyanobacterial biomass, as antimicrobial agents. The ability of these nanoparticles to inhibit the bacterial growth of *Staphylococcus aureus* and *Escherichia coli* reflects their potential application in biomedical and pharmacological fields. Finally, the present research lays a solid foundation for the future development of metal nanoparticles via biological methods, highlighting the value of EPSs as synthesis and stabilization agents and paving the way for practical applications in medicine, biotechnology, and pharmacology.

## 5. Conclusions

In the synthesis of metallic NPs, the exopolysaccharides secreted by cyanobacteria in the logarithmic growth phase are more efficient in the biosynthesis of Nps and have greater bacterial growth inhibition than those produced with the biomass extract. The most important operational factors in the synthesis of NPs are the reaction time and the algae-to-metal ratio, which vary depending on the bacteria to be inhibited; for Gram-negative bacteria such as *E. coli*, less time (almost 3 days) and a ratio of 8% EPS/$AgNO_3$ solution at the time of synthesis of the NPs are needed. In comparison, Gram-positive bacteria (*S. aureus*) require more time (4.5 days) and a lower ratio of EPS/$AgNO_3$ solution (4.5%), with an approximate concentration of 3 mM $AgNO_3$ and a speed of approximately 240 rpm in both cases.

Characterization of the AgNPs by UV–VIS revealed that the wavelength for maximum absorption was 427 nm for AgNP006 and 438 nm for AgNP011, which is in the wavelength range of AgNP formation. The EDX spectrum confirmed the presence of silver metal, with the highest peak at 3 keV and silver emission peaks of more than 74% present in both AgNP samples, indicating high purity and intensity at the time of synthesis.

**Author Contributions:** Conceptualization, J.B.G.-M. and A.F.B.-S.; methodology, M.L.R.-G. and G.L.L.-B.; software, A.F.B.-S. and N.A.U.-S.; validation, A.F.B.-S. and M.L.R.-G.; formal analysis, M.L.R.-G., G.L.L.-B. and J.B.G.-M.; investigation, M.L.R.-G.; resources, A.F.B.-S. and J.B.G.-M.; data curation, N.A.U.-S. and G.L.L.-B.; writing—original draft preparation, G.L.L.-B. and M.L.R.-G.; writing—review and editing, J.B.G.-M. and G.L.L.-B.; visualization, A.F.B.-S.; supervision, G.L.L.-B.; project administration, J.B.G.-M.; funding acquisition, A.F.B.-S. and N.A.U.-S. All authors have read and agreed to the published version of the manuscript.

**Funding:** This study received financial support through grants from Universidad Francisco de Paula Santander (Colombia) (FINU 011-2023), the Ministry of Science and Technology of Colombia, and the Colombian Institute of Educational Credit and Technical Studies Abroad (MINCIENCIAS-ICETEX) under the project titled "FOTOLIX" with the ID 2023-0686.

**Institutional Review Board Statement:** Not applicable.

**Informed Consent Statement:** Not applicable.

**Data Availability Statement:** Data are contained within the article.

**Acknowledgments:** We would like to express our sincere gratitude to Universidad Francisco de Paula Santander (Colombia) for providing the equipment for this research. We also thank the Colombian Ministry of Science, Technology, and Innovation MINCIENCIAS for supporting the national Ph.D. doctorates through the Francisco José de Caldas scholarship program.

**Conflicts of Interest:** The authors declare no conflicts of interest.

## References

1. Rónavári, A.; Igaz, N.; Adamecz, D.I.; Szerencsés, B.; Molnar, C.; Kónya, Z.; Pfeiffer, I.; Kiricsi, M. Green Silver and Gold Nanoparticles: Biological Synthesis Approaches and Potentials for Biomedical Applications. *Molecules* **2021**, *26*, 844. [CrossRef]
2. Ying, S.; Guan, Z.; Ofoegbu, P.C.; Clubb, P.; Rico, C.; He, F.; Hong, J. Green Synthesis of Nanoparticles: Current Developments and Limitations. *Environ. Technol. Innov.* **2022**, *26*, 102336. [CrossRef]
3. Iravani, S.; Korbekandi, H.; Mirmohammadi, S.V.; Zolfaghari, B. Synthesis of Silver Nanoparticles: Chemical, Physical and Biological Methods. *Res. Pharm. Sci.* **2014**, *9*, 385.
4. Mittal, A.K.; Chisti, Y.; Banerjee, U.C. Synthesis of Metallic Nanoparticles Using Plant Extracts. *Biotechnol. Adv.* **2013**, *31*, 346–356. [CrossRef]
5. Singh, P.; Kim, Y.J.; Zhang, D.; Yang, D.C. Biological Synthesis of Nanoparticles from Plants and Microorganisms. *Trends Biotechnol.* **2016**, *34*, 588–599. [CrossRef]
6. Patel, V.; Berthold, D.; Puranik, P.; Gantar, M. Screening of Cyanobacteria and Microalgae for Their Ability to Synthesize Silver Nanoparticles with Antibacterial Activity. *Biotechnol. Rep.* **2014**, *5*, 112–119. [CrossRef]
7. Barajas-Solano, A.F. Optimization of Phycobiliprotein Solubilization from a Thermotolerant *Oscillatoria* sp. *Processes* **2022**, *10*, 836. [CrossRef]
8. Castellanos-Estupiñan, M.; Carrillo-Botello, A.; Rozo-Granados, L.; Becerra-Moreno, D.; García-Martínez, J.; Urbina-Suarez, N.; López-Barrera, G.; Barajas-Solano, A.; Bryan, S.; Zuorro, A. Removal of Nutrients and Pesticides from Agricultural Runoff Using Microalgae and Cyanobacteria. *Water* **2022**, *14*, 558. [CrossRef]
9. Vergel-Suarez, A.H.; García-Martínez, J.B.; López-Barrera, G.L.; Barajas-Solano, A.F.; Zuorro, A. Impact of Biomass Drying Process on the Extraction Efficiency of C-Phycoerythrin. *BioTech* **2023**, *12*, 30. [CrossRef] [PubMed]
10. Sharma, D.; Kanchi, S.; Bisetty, K. Biogenic Synthesis of Nanoparticles: A Review. *Arab. J. Chem.* **2019**, *12*, 3576–3600. [CrossRef]
11. Ebrahiminezhad, A.; Bagheri, M.; Taghizadeh, S.M.; Berenjian, A.; Ghasemi, Y. Biomimetic Synthesis of Silver Nanoparticles Using Microalgal Secretory Carbohydrates as a Novel Anticancer and Antimicrobial. *Adv. Nat. Sci. Nanosci. Nanotechnol.* **2016**, *7*, 015018. [CrossRef]
12. Priyadarshini, S.S.; Sethi, S.; Rout, S.; Mishra, P.M.; Pradhan, N. Green Synthesis of Microalgal Biomass-Silver Nanoparticle Composite Showing Antimicrobial Activity and Heterogenous Catalysis of Nitrophenol Reduction. *Biomass Convers. Biorefin* **2023**, *13*, 7783–7795. [CrossRef]
13. Sathishkumar, R.S.; Sundaramanickam, A.; Srinath, R.; Ramesh, T.; Saranya, K.; Meena, M.; Surya, P. Green Synthesis of Silver Nanoparticles by Bloom Forming Marine Microalgae Trichodesmium Erythraeum and Its Applications in Antioxidant, Drug-Resistant Bacteria, and Cytotoxicity Activity. *J. Saudi Chem. Soc.* **2019**, *23*, 1180–1191. [CrossRef]
14. da Silva Ferreira, V.; ConzFerreira, M.E.; Lima, L.M.T.R.; Frasés, S.; de Souza, W.; Sant'Anna, C. Green Production of Microalgae-Based Silver Chloride Nanoparticles with Antimicrobial Activity against Pathogenic Bacteria. *Enzyme Microb. Technol.* **2017**, *97*, 114–121. [CrossRef]
15. Mandhata, C.P.; Sahoo, C.R.; Mahanta, C.S.; Padhy, R.N. Isolation, Biosynthesis and Antimicrobial Activity of Gold Nanoparticles Produced with Extracts of Anabaena Spiroides. *Bioprocess. Biosyst. Eng.* **2021**, *44*, 1617–1626. [CrossRef]

16. Zuorro, A.; Leal-Jerez, A.G.; Morales-Rivas, L.K.; Mogollón-Londoño, S.O.; Sanchez-Galvis, E.M.; García-Martínez, J.B.; Barajas-Solano, A.F. Enhancement of Phycobiliprotein Accumulation in Thermotolerant *Oscillatoria* Sp. through Media Optimization. *ACS Omega* **2021**, *6*, 10527. [CrossRef]
17. Vega-Jiménez, A.L.; Vázquez-Olmos, A.R.; Acosta-Gío, E.; Antonio Álvarez-Pérez, M. In Vitro Antimicrobial Activity Evaluation of Metal Oxide Nanoparticles. In *Nanoemulsions—Properties, Fabrications and Applications*; IntechOpen: London, UK, 2019.
18. Roychoudhury, P.; Gopal, P.K.; Paul, S.; Pal, R. Cyanobacteria Assisted Biosynthesis of Silver Nanoparticles—A Potential Antileukemic Agent. *J. Appl. Phycol.* **2016**, *28*, 3387–3394. [CrossRef]
19. Vanlalveni, C.; Rajkumari, K.; Biswas, A.; Adhikari, P.P.; Lalfakzuala, R.; Rokhum, L. Green Synthesis of Silver Nanoparticles Using Nostoc Linckia and Its Antimicrobial Activity: A Novel Biological Approach. *Bionanoscience* **2018**, *8*, 624–631. [CrossRef]
20. Dubois, M.; Gilles, K.A.; Hamilton, J.K.; Rebers, P.A.; Smith, F. Colorimetric Method for Determination of Sugars and Related Substances. *Anal. Chem.* **1956**, *28*, 350–356. [CrossRef]
21. Waterborg, J.H. The Lowry Method for Protein Quantitation. In *The Protein Protocols Handbook*; Walker, J.M., Ed.; Humana Press: Totowa, NJ, USA, 2009; pp. 7–10. ISBN 978-1-59745-198-7.
22. Frings, C.S.; Dunn, R.T. A Colorimetric Method for Determination of Total Serum Lipids Based on the Sulfo-Phospho-Vanillin Reaction. *Am. J. Clin. Pathol.* **1970**, *53*, 89–91. [CrossRef]
23. Barman, K.; Chowdhury, D.; Baruah, P.K. Bio-Synthesized Silver Nanoparticles Using Zingiber Officinale Rhizome Extract as Efficient Catalyst for the Degradation of Environmental Pollutants. *Inorg. Nano-Metal Chem.* **2020**, *50*, 57–65. [CrossRef]
24. Tugarova, A.V.; Mamchenkova, P.V.; Dyatlova, Y.A.; Kamnev, A.A. FTIR and Raman Spectroscopic Studies of Selenium Nanoparticles Synthesised by the Bacterium Azospirillum Thiophilum. *Spectrochim. Acta A Mol. Biomol. Spectrosc.* **2018**, *192*, 458–463. [CrossRef] [PubMed]
25. Akter, S.; Huq, M.A. Biologically Rapid Synthesis of Silver Nanoparticles by *Sphingobium* sp. MAH-11$^{T}$ and Their Antibacterial Activity and Mechanisms Investigation against Drug-Resistant Pathogenic Microbes. *Artif. Cells Nanomed. Biotechnol.* **2020**, *48*, 672–682. [CrossRef] [PubMed]
26. Kristinaitytė, K.; Dagys, L.; Kausteklis, J.; Klimavicius, V.; Doroshenko, I.; Pogorelov, V.; Valevičienė, N.R.; Balevicius, V. NMR and FTIR Studies of Clustering of Water Molecules: From Low-Temperature Matrices to Nano-Structured Materials Used in Innovative Medicine. *J. Mol. Liq.* **2017**, *235*, 1–6. [CrossRef]
27. Bakirdere, S.; Yilmaz, M.T.; Tornuk, F.; Keyf, S.; Yilmaz, A.; Sagdic, O.; Kocabas, B. Molecular Characterization of Silver–Stearate Nanoparticles (AgStNPs): A Hydrophobic and Antimicrobial Material against Foodborne Pathogens. *Food Res. Int.* **2015**, *76*, 439–448. [CrossRef]
28. Venkataesan Kumari, B.; Mani, R.; Asokan, B.R.; Balakrishnan, K.; Ramasamy, A.; Parthasarathi, R.; Kandasamy, C.; Govindaraj, R.; Vijayakumar, N.; Vijayakumar, S. Green Synthesised Silver Nanoparticles Using Anoectochilus Elatus Leaf Extract: Characterisation and Evaluation of Antioxidant, Anti-Inflammatory, Antidiabetic, and Antimicrobial Activities. *J. Compos. Sci.* **2023**, *7*, 453. [CrossRef]
29. Yılmaz Öztürk, B.; Yenice Gürsu, B.; Dağ, İ. Antibiofilm and Antimicrobial Activities of Green Synthesized Silver Nanoparticles Using Marine Red Algae Gelidium Corneum. *Process Biochem.* **2020**, *89*, 208–219. [CrossRef]
30. Garzón, M.G. Therapeutic Uses of Nanomaterials and Nanoparticles. *Fund. Univ. Cienc. Salud-FUCS* **2019**, *28*, 5–11.
31. Kohsari, I.; Mohammad-Zadeh, M.; Minaeian, S.; Rezaee, M.; Barzegari, A.; Shariatinia, Z.; Koudehi, M.F.; Mirsadeghi, S.; Pourmortazavi, S.M. In Vitro Antibacterial Property Assessment of Silver Nanoparticles Synthesized by Falcaria Vulgaris Aqueous Extract against MDR Bacteria. *J. Solgel Sci. Technol.* **2019**, *90*, 380–389. [CrossRef]
32. Huq, M.A.; Akter, S. Biosynthesis, Characterization and Antibacterial Application of Novel Silver Nanoparticles against Drug Resistant Pathogenic Klebsiella Pneumoniae and Salmonella Enteritidis. *Molecules* **2021**, *26*, 5996. [CrossRef]
33. Maher, C.; Hassan, K.A. The Gram-Negative Permeability Barrier: Tipping the Balance of the in and the Out. *mBio* **2023**, *14*, e0120523. [CrossRef] [PubMed]
34. Manosalva, N.; Tortella, G.; Cristina Diez, M.; Schalchli, H.; Seabra, A.B.; Durán, N.; Rubilar, O. Green Synthesis of Silver Nanoparticles: Effect of Synthesis Reaction Parameters on Antimicrobial Activity. *World J. Microbiol. Biotechnol.* **2019**, *35*, 88. [CrossRef] [PubMed]
35. Vidovic, S.; Elder, J.; Medihala, P.; Lawrence, J.R.; Predicala, B.; Zhang, H.; Korber, D.R. ZnO Nanoparticles Impose a Panmetabolic Toxic Effect Along with Strong Necrosis, Inducing Activation of the Envelope Stress Response in Salmonella Enterica Serovar Enteritidis. *Antimicrob. Agents Chemother.* **2015**, *59*, 3317–3328. [CrossRef] [PubMed]
36. Soria, M.V.C. Nanosistemas Empleados En Terapia Antibiótica. Ph.D. Thesis, Universidad de Sevilla, Sevilla, Spain, 2016; pp. 1–40.
37. Shaaban, M.; El-Mahdy, A.M. Biosynthesis of Ag, Se, and ZnO Nanoparticles with Antimicrobial Activities against Resistant Pathogens Using Waste Isolate *Streptomyces Enissocaesilis*. *IET Nanobiotechnol* **2018**, *12*, 741–747. [CrossRef]
38. Gao, J.; Na, H.; Zhong, R.; Yuan, M.; Guo, J.; Zhao, L.; Wang, Y.; Wang, L.; Zhang, F. One Step Synthesis of Antimicrobial Peptide Protected Silver Nanoparticles: The Core-Shell Mutual Enhancement of Antibacterial Activity. *Colloids Surf. B Biointerfaces* **2020**, *186*, 110704. [CrossRef]
39. El-Naggar, N.E.A.; Hussein, M.H.; Shaaban-Dessuuki, S.A.; Dalal, S.R. Production, Extraction and Characterization of Chlorella Vulgaris Soluble Polysaccharides and Their Applications in AgNPs Biosynthesis and Biostimulation of Plant Growth. *Sci. Rep.* **2020**, *10*, 3011. [CrossRef]

40. Singh, A.; Gaud, B.; Jaybhaye, S. Optimization of Synthesis Parameters of Silver Nanoparticles and Its Antimicrobial Activity. *Mater. Sci. Energy Technol.* **2020**, *3*, 232–236. [CrossRef]
41. Tufail, S.; Liaqat, I.; Ali, S.; Ulfat, M.; Shafi, A.; Sadiqa, A.; Iqbal, R.; Ahsan, F. Bacillus licheniformis (MN900686) Mediated Synthesis, Characterization and Antimicrobial Potential of Silver Nanoparticles. *J. Oleo Sci.* **2022**, *71*, ess21441. [CrossRef] [PubMed]
42. Wypij, M.; Czarnecka, J.; Świecimska, M.; Dahm, H.; Rai, M.; Golinska, P. Synthesis, Characterization and Evaluation of Antimicrobial and Cytotoxic Activities of Biogenic Silver Nanoparticles Synthesized from Streptomyces Xinghaiensis OF1 Strain. *World J. Microbiol. Biotechnol.* **2018**, *34*, 23. [CrossRef]
43. Rai, A.; Pinto, S.; Velho, T.R.; Ferreira, A.F.; Moita, C.; Trivedi, U.; Evangelista, M.; Comune, M.; Rumbaugh, K.P.; Simões, P.N.; et al. One-Step Synthesis of High-Density Peptide-Conjugated Gold Nanoparticles with Antimicrobial Efficacy in a Systemic Infection Model. *Biomaterials* **2016**, *85*, 99–110. [CrossRef]
44. Niranjan, R.; Zafar, S.; Lochab, B.; Priyadarshini, R. Synthesis and Characterization of Sulfur and Sulfur-Selenium Nanoparticles Loaded on Reduced Graphene Oxide and Their Antibacterial Activity against Gram-Positive Pathogens. *Nanomaterials* **2022**, *12*, 191. [CrossRef] [PubMed]
45. Medina Cruz, D.; Mi, G.; Webster, T.J. Synthesis and Characterization of Biogenic Selenium Nanoparticles with Antimicrobial Properties Made by *Staphylococcus Aureus*, Methicillin-resistant *Staphylococcus Aureus* (MRSA), *Escherichia Coli*, and *Pseudomonas Aeruginosa*. *J. Biomed. Mater. Res. A* **2018**, *106*, 1400–1412. [CrossRef] [PubMed]
46. Dakal, T.C.; Kumar, A.; Majumdar, R.S.; Yadav, V. Mechanistic Basis of Antimicrobial Actions of Silver Nanoparticles. *Front. Microbiol.* **2016**, *7*, 231711. [CrossRef] [PubMed]
47. You, C.; Han, C.; Wang, X.; Zheng, Y.; Li, Q.; Hu, X.; Sun, H. The Progress of Silver Nanoparticles in the Antibacterial Mechanism, Clinical Application and Cytotoxicity. *Mol. Biol. Rep.* **2012**, *39*, 9193–9201. [CrossRef]
48. Nikaeen, G.; Yousefinejad, S.; Rahmdel, S.; Samari, F.; Mahdavinia, S. Central Composite Design for Optimizing the Biosynthesis of Silver Nanoparticles Using Plantago Major Extract and Investigating Antibacterial, Antifungal and Antioxidant Activity. *Sci. Rep.* **2020**, *10*, 9642. [CrossRef]
49. Elshafei, A.M.; Othman, A.M.; Elsayed, M.A.; Al-Balakocy, N.G.; Hassan, M.M. Green Synthesis of Silver Nanoparticles Using Aspergillus Oryzae NRRL447 Exogenous Proteins: Optimization via Central Composite Design, Characterization and Biological Applications. *Environ. Nanotechnol. Monit. Manag.* **2021**, *16*, 100553. [CrossRef]
50. Padilla-Cruz, A.L.; Garza-Cervantes, J.A.; Vasto-Anzaldo, X.G.; García-Rivas, G.; León-Buitimea, A.; Morones-Ramírez, J.R. Synthesis and Design of Ag–Fe Bimetallic Nanoparticles as Antimicrobial Synergistic Combination Therapies against Clinically Relevant Pathogens. *Sci. Rep.* **2021**, *11*, 5351. [CrossRef]
51. Adibah, N.; Firdianti, B.E.; Suprapto, S. Synthesis of Silver Nanoparticles Using Response Surface Methodology. *J. Nano-Electron. Phys.* **2023**, *15*, 03001-1–03001-4. [CrossRef]
52. Aletayeb, P.; Ghadam, P.; Mohammadi, P. Green Synthesis of $AgCl/Ag_3PO_4$ Nanoparticle Using Cyanobacteria and Assessment of Its Antibacterial, Colorimetric Detection of Heavy Metals and Antioxidant Properties. *IET Nanobiotechnol.* **2020**, *14*, 707–713. [CrossRef]
53. İspirli, H.; Sagdic, O.; Dertli, E. Synthesis of Silver Nanoparticles Prepared with a Dextran-Type Exopolysaccharide from *Weissella Cibaria* MED17 with Antimicrobial Functions. *Prep. Biochem. Biotechnol.* **2021**, *51*, 112–119. [CrossRef]
54. Nilavukkarasi, M.; Vijayakumar, S.; Prathip Kumar, S. Biological Synthesis and Characterization of Silver Nanoparticles with Capparis Zeylanica L. Leaf Extract for Potent Antimicrobial and Anti Proliferation Efficiency. *Mater. Sci. Energy Technol.* **2020**, *3*, 371–376. [CrossRef]
55. Hamouda, R.A.; Hussein, M.H.; Elhadary, A.M.A.; Abuelmagd, M.A. Extruded Polysaccharide/Protein Matrix from Arthrospira Platensis Cultures Mediated Silver Nanoparticles Biosynthesis and Capping. *Appl. Nanosci.* **2020**, *10*, 3839–3855. [CrossRef]
56. Hanna, A.L.; Hamouda, H.M.; Goda, H.A.; Sadik, M.W.; Moghanm, F.S.; Ghoneim, A.M.; Alenezi, M.A.; Alnomasy, S.F.; Alam, P.; Elsayed, T.R. Biosynthesis and Characterization of Silver Nanoparticles Produced by *Phormidium Ambiguum* and *Desertifilum Tharense* Cyanobacteria. *Bioinorg. Chem. Appl.* **2022**, *2022*, 9072508. [CrossRef] [PubMed]
57. Karageorgou, D.; Zygouri, P.; Tsakiridis, T.; Hammami, M.A.; Chalmpes, N.; Subrati, M.; Sainis, I.; Spyrou, K.; Katapodis, P.; Gournis, D.; et al. Green Synthesis and Characterization of Silver Nanoparticles with High Antibacterial Activity Using Cell Extracts of Cyanobacterium *Pseudanabaena/Limnothrix* sp. *Nanomaterials* **2022**, *12*, 2296. [CrossRef] [PubMed]
58. Sahoo, C.R.; Swain, S.; Luke, A.M.; Paidesetty, S.K.; Padhy, R.N. Biogenic Synthesis of Silver-Nanoparticles with the Brackish Water Cyanobacterium *Nostoc Sphaeroides* and Assessment of Antibacterial Activity against Urinary Tract Infecting Bacteria. *J. Taibah Univ. Sci.* **2021**, *15*, 805–813. [CrossRef]
59. Guna Swetha, K.; Sujatha, E.; Thrimothy, D.; Mamatha, R. Characterization, in Vitro Cytotoxic and Antibacterial Exploitation of Green Synthesized Freshwater Cyanobacterial Silver Nanoparticles. *J. Appl. Pharm. Sci.* **2020**, *10*, 088–098. [CrossRef]
60. Younis, N.S.; Mohamed, M.E.; El Semary, N.A. Green Synthesis of Silver Nanoparticles by the Cyanobacteria Synechocystis Sp.: Characterization, Antimicrobial and Diabetic Wound-Healing Actions. *Mar. Drugs* **2022**, *20*, 56. [CrossRef]